Journal of Thermal Analysis and Calorimetry (2021) 143:3849–3866
https://doi.org/10.1007/s10973-020-09324-4

Study of thermal performance of a ferrofluid with multivariable dependence viscosity within a wavy duct with external magnetic force

Hamid Kazemi Moghadam[1] · Saeed Samadzadeh Baghbani[2] · Houman Babazadeh[3,4]

Received: 14 September 2019 / Accepted: 11 January 2020 / Published online: 27 January 2020

Abstract
Ferrofluids are type of colloidal systems which are known as an important group of smart materials. Their physical properties adaptively change with magnetic strength. These characteristics of ferrofluid must be applied for improving the efficiency. In this work, thermal performance of a type of ferrofluid with a viscosity correlation dependence on temperature, magnetic field and volume fraction was scrutinized. FVM is applied for solving momentum, conservation and heat transfer equation. To consider the effect of solid part in thermal behavior of system, the conjugate heat transfer was considered. The wire is placed in the bottom of channel, and the equation of non-uniform external magnetic field is defined as user function. The results indicated in a comparison of studied parameters as non-dimensional variables, it is demonstrated magnetic number and wave amplitude result in the maximum impact on improving Nu and the worst impact on friction coefficient and pressure loss correspondence to volume fraction and Reynolds number. The results also predicted significant changes in viscosity under influence of effective parameters, especially Kelvin force.

Keywords Ferrofluid · Heat transfer augmentation · Magnetic field · Nusselt · Multivariable dependence viscosity

Introduction

Nanotechnology is one of the most brilliant areas in fluid mechanics that attract the researchers due to its greater capability. Nanomaterial is the new invent which is achieved by applying nano powders [1–11]. The special features of nanofluid can be used in thermal and heat enhancement applications due to the flow field changes under the influence of magnetic fields [12–26]. Variety of researches were done in this field [27–38]. In one of the new investigations, Taslimifar et al. [39] reported in their study the using of nanomaterial in steady with using Kelvin forces. Gandomkar et al. [40] investigated pulsating ferrofluid heat pipe, to discover the best design between three different studied cases of magnetic field. Khoshmehr et al. [41] scrutinized the influences of combined ferrofluid and magnetic field in the boiling phenomena. Their experiment revealed that applying magnetic force led to enhancement in the boiling heat flux. Ahmad and Iqbal [42] presented a study on ferrofluid with temperature dependence viscosity affected by no-slip condition. Their results showed the concentration enhanced by enhancing viscous dissipation and Schmidt number. Strek and Jopek [43] investigated ferrofluid heat transfer under the impact of Kelvin forces. Shima and Philip [44] illustrated from their study on magnetic field effect on thermophysical properties that these properties could be changed significantly by changing magnetic field parameters. Simulation-based demonstrations help the researchers to find best configuration [45–64]. Gavili et al. [65] investigation on thermal conductivity of ferrofluid revealed that applying a magnetic source significantly increased thermal conductivity. Mehrali et al.'s [66] study on entropy generation of hybrid graphene–magnetite nanomaterial illustrated the irreversibility reduced significantly compared to raw H_2O. Abdel-wahed [67] investigation on ferrofluid predicted

✉ Houman Babazadeh
houman.babazadeh@tdtu.edu.vn

1 Department of Mechanical Engineering, Babol Noshirvani University of Technology, Babol, Iran

2 Department of Mechanical Engineering, Islamic Azad University, South Tehran Branch, Tehran, Iran

3 Department for Management of Science and Technology Development, Ton Duc Thang University, Ho Chi Minh City, Vietnam

4 Faculty of Environment and Labour Safety, Ton Duc Thang University, Ho Chi Minh City, Vietnam

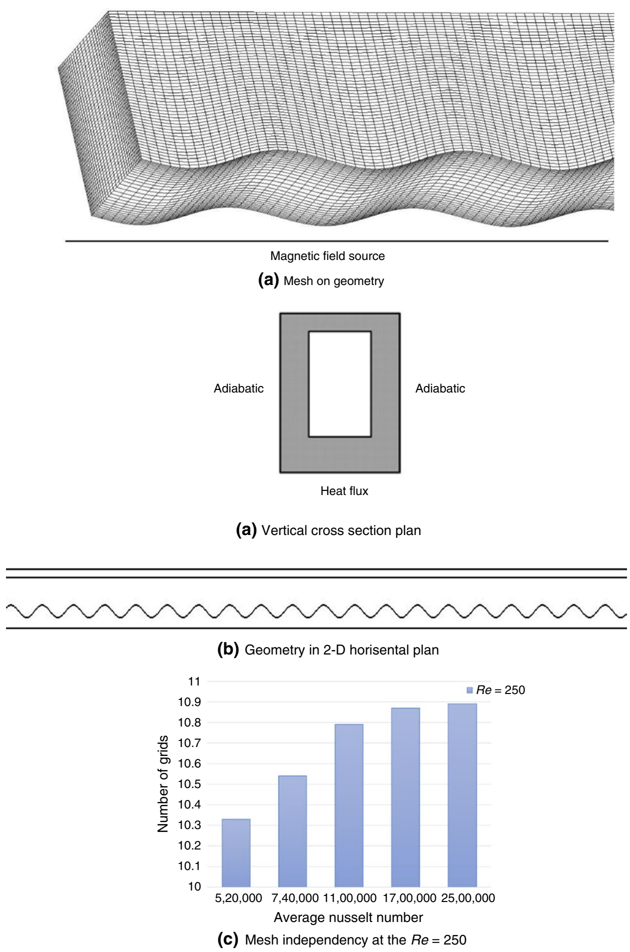

Fig. 1 Geometry and mesh

that nano size particles improved the Nu and decreased the surface shear stress, whereas curvature of the tube caused negative impact on Nu. Various numerical methods exist to evaluate performance of system [68–88]. Krishna Shah and Khandekar [89] also conducted a study on potential of ferrofluids for heat transfer augmentation, via numerical simulations. They found that higher volume fraction loading and magnetic fields applying resulted in better efficiency and local Nusselt number observed to reach a significant increase higher than no magnetic field case. Heat transfer efficiency of heat pipe with three different working fluids was studied by Hao et al. [90]. They found that startup efficiency of acetone-filled heat pipe is the best and friction of acetone-filled heat pipes showed the lowest efficiency. Sheikholeslami et al. [91] scrutinized the impact of external force on ferrofluid heat transfer argumentation in ribbed channel. They studied different parameters such as magnetic sources arrangement and their magnitude on improving heat transfer from the channel.

In this study, changes in thermophysical parameters of a ferrofluid with a multivariable dependence viscosity in a wavy microchannel are presented. The impacts of parameters such as R_e, wave amplitude, magnetic number and concentration on heat transfer coefficient, Nu, f on the domain have been investigated, and their influences are compared together.

Governing equation

The schematic of the considered geometry for the problem, a wavy microchannel with current-carrying wire as external source of magnetic field, and some of the boundary conditions in two horizontal and vertical cross sections are shown in Fig. 1. Equations of steady-state conditions are as follows [91]:

$$\nabla \cdot \rho_{\mathrm{nf}} \vec{U} = 0 \tag{1}$$

$$\frac{D\vec{U}}{Dt} = -\frac{1}{\rho_{\mathrm{nf}}} \nabla P + \nu_{\mathrm{nf}} \nabla^2 \vec{U} + \frac{\mu_0}{\rho_{\mathrm{nf}}} M \nabla \vec{H} + \vec{F}_{\mathrm{L}} \tag{2}$$

The term $\frac{\mu_0}{\rho} M \nabla \vec{H}$ is representative of magnetic force, and F_{L} is Lorentz force consequent of the MHD.

Equations with considering FHD can be presented as follows [91–93]:

$$\rho_{\mathrm{nf}} \left[\frac{\partial v}{\partial t} + w \frac{\partial v}{\partial z} + v \frac{\partial v}{\partial y} + u \frac{\partial v}{\partial x} \right] = -\nabla P + \mu_{\mathrm{nf}} \left(\nabla^2 v \right) + \mu_0 M \frac{\partial \vec{H}}{\partial y} - \sigma_{\mathrm{nf}} B_{\mathrm{x}}^2 u + \sigma_{\mathrm{nf}} B_{\mathrm{x}} B_{\mathrm{y}} u \tag{3}$$

$$\rho_{\mathrm{nf}} \left[\frac{\partial u}{\partial t} + w \frac{\partial u}{\partial z} + v \frac{\partial u}{\partial y} + u \frac{\partial u}{\partial x} \right] = -\nabla P + \mu_{\mathrm{nf}} \left(\nabla^2 u \right) + \mu_0 M \frac{\partial \vec{H}}{\partial x} - \sigma_{\mathrm{nf}} B_{\mathrm{y}}^2 u + \sigma_{\mathrm{nf}} B_{\mathrm{x}} B_{\mathrm{y}} \upsilon \tag{4}$$

$$\frac{\partial w}{\partial y} + \frac{\partial v}{\partial y} + \frac{\partial u}{\partial x} = 0 \tag{5}$$

$$\begin{aligned}(\rho C_p)_{nf}\left(w\frac{\partial T}{\partial z} + v\frac{\partial T}{\partial y} + u\frac{\partial T}{\partial x}\right) &= K_{nf}\left(\frac{\partial^2 T}{\partial y^2} + \frac{\partial^2 T}{\partial z^2} + \frac{\partial^2 T}{\partial x^2}\right) \\ &+ \sigma_{nf}(\mathrm{uB_y} - v\mathrm{B_x})^2 + \mu_{nf}\left(2\left(\frac{\partial u}{\partial x}\right)^2 + 2\left(\frac{\partial u}{\partial y}\right)^2 + 2\left(\frac{\partial u}{\partial z}\right)^2 + CurlV\right) \\ &- \mu_0 T\frac{\partial M}{\partial x}\left(u\frac{\partial \bar{H}}{\partial x} + v\frac{\partial \bar{H}}{\partial y} + w\frac{\partial \bar{H}}{\partial z}\right)\end{aligned} \tag{6}$$

The terms $\mu_0 M\frac{\partial \vec{H}}{\partial x}$ and $\mu_0 M\frac{\partial \vec{H}}{\partial y}$ show the magnetic force effect. The terms $\sigma_{nf}B_y^2 u + \sigma_{nf}B_x B_y v$ and $\sigma_{nf}B_x^2 u + \sigma_{nf}B_x B_y u$ in (4) and (5) are representatives of Lorentz force. For the different magnetization M, the following equation is derived [91]:

$$M = (T_c' - T)\bar{H}K' \tag{7}$$

H_x and H_y are defined as [91]:

$$\begin{aligned}H_x &= (x-a)\frac{1}{2\pi}\frac{\gamma}{(a-x)^2-(b-y)^2}, \\ H_y &= (b-y)\frac{1}{2\pi}\frac{\gamma}{(a-x)^2-(b-y)^2}\end{aligned} \tag{8}$$

Here (a, b) is the coordinate of wire. H as the magnetic field intensity was defined as follows [91]:

$$H = \sqrt{Hx^2 + Hy^2} = \frac{\gamma}{2\pi(x-a)^2-(y-b)^2} \tag{9}$$

Magnetic numbers ($\mathrm{Mn_f}$) and Hartmann as two important parameters appearing in magnetic problems are defined as follows:

$$\mathrm{Mn_f} = \frac{h^2\mu_0 kH^2}{v_{nf}^2\rho_{nf}} = \frac{h^2 BM}{v_{nf}^2\rho_{nf}} \tag{10}$$

$$\mathrm{Ha} = B_y D\sqrt{\frac{\sigma_{nf}}{\mu_{nf}}} \tag{11}$$

where h is the microchannel height.

$$\mathrm{Mn_f} = \frac{h^2\mu_0\chi H_0^2}{v_{nf}^2\rho_{nf}} \tag{12}$$

where B_0 is the highest value of magnetic field and χ is magnetic susceptibility.

$$R_e = \frac{VD}{v_{nf}}\mathrm{Nu_{loc}} = \frac{hl}{K_{nf}} \quad C_f = \frac{\tau_w}{\frac{1}{2}\rho_{nf}U_{in}^2} \tag{13}$$

$$\begin{aligned}(\rho C_p)_{nf} &= (\rho C_p)_f(1-\varphi) + (\rho C_p)_f\varphi \\ \rho_{nf} &= \rho_f(1-\varphi) + \rho_s\varphi\end{aligned} \tag{14}$$

$$\alpha_{nf} = \frac{K_{nf}}{(\rho C_p)_{nf}} \tag{15}$$

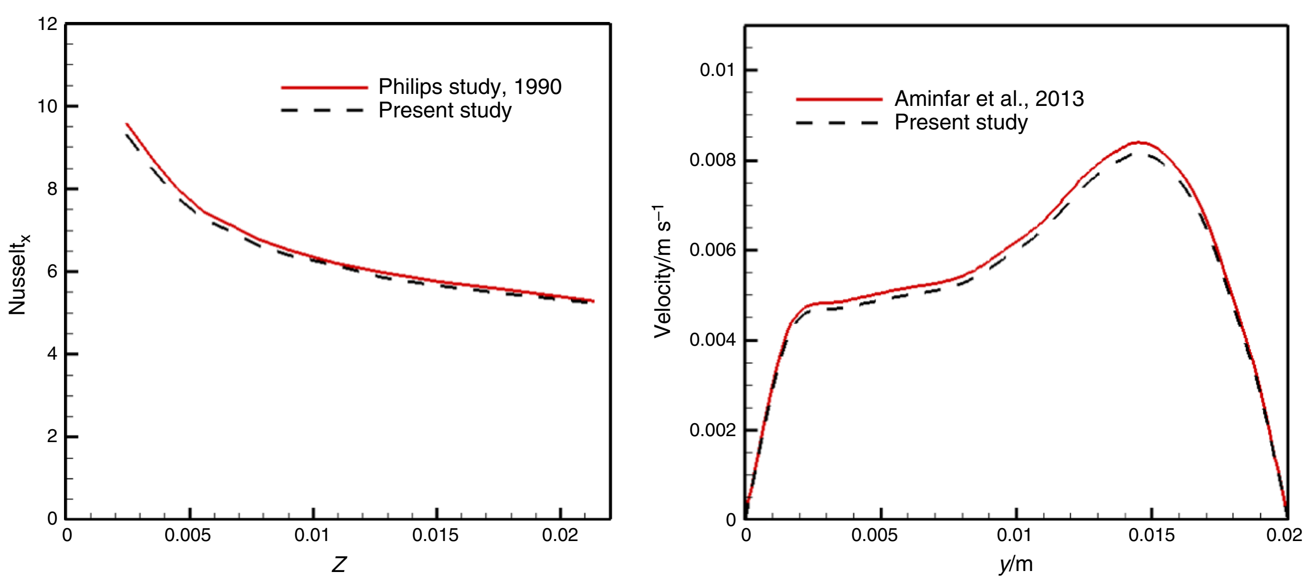

(a) Validation of nusselt number in channel with theoretical results [93]

(b) Validation of magnetic field in channel with aminifar et al. [94]

Fig. 2 Validation of Nusselt number and magnetic fields effect in a channel

Table 1 Quantities of parameters in simulation

K_f /W m K^{-1}	Thermal conductivity of fluid (pure water)	0.6
ρ_f/kg m^{-3}	Fluid density	1050
ρ_p/kg m^{-3}	Particle density	4600
μ_0/N A^{-2}	Magnetic permeability of vacuum	$4\pi \times 10^{-7}$
χ/m^3/kg^{-1}	Magnetic susceptibility	3×10^{-6}
K_s/W m K^{-1}	thermal conductivity of nano particles (Fe_3O_4)	6
σ_f/Ω m^{-1}	Fluid electrical conductivity	0.05
σ_s/Ω m^{-1}	Nano-particles electrical conductivity	25,000
b. Geometry features		
L/m	Length of channel	0.01
B/μm	Depth of channel	250
H/mm	Height of channel	0.5
h/μm	Wave amplitude	25, 50, 75
c. Boundary conditions		
Internal-walls	Conjugate	
Down-wall	Heat flux (100 w cm^{-2})	
Upper wall and right and left Out-walls	Adiabatic	

$$\frac{K_{nf}}{K_f} = \frac{K_s + 2K_f - 2\varphi(K_f - K_s)}{K_s + 2K_f - \varphi(K_f - K_s)} \tag{16}$$

Also σ_{nf} is defined (see for details [91]) as:

$$\frac{\sigma_{nf}}{\sigma_f} = 1 + \left[3\varphi\left(\frac{\sigma_s}{\sigma_f} - 1\right)\right]\frac{1}{\left(\frac{\sigma_s}{\sigma_f} + 2\right) - \varphi\left(-1 + \frac{\sigma_s}{\sigma_f}\right)} \tag{17}$$

The viscosity of nanofluid considered from correlations is extracted from experimental data proposed by nonlinear fitting by Wang et al. [92]. The ranges of volume fraction and temperature were considered 0.5–5% and 293–333 K, respectively, and the final equation for viscosity that is considered in this study is given as follows:

$$\mu_{nf} = (316.0629 - 27886.4807\phi^2 + 0.035H^2 + 4263.02\phi + 3.1H)e^{-0.02T} \tag{18}$$

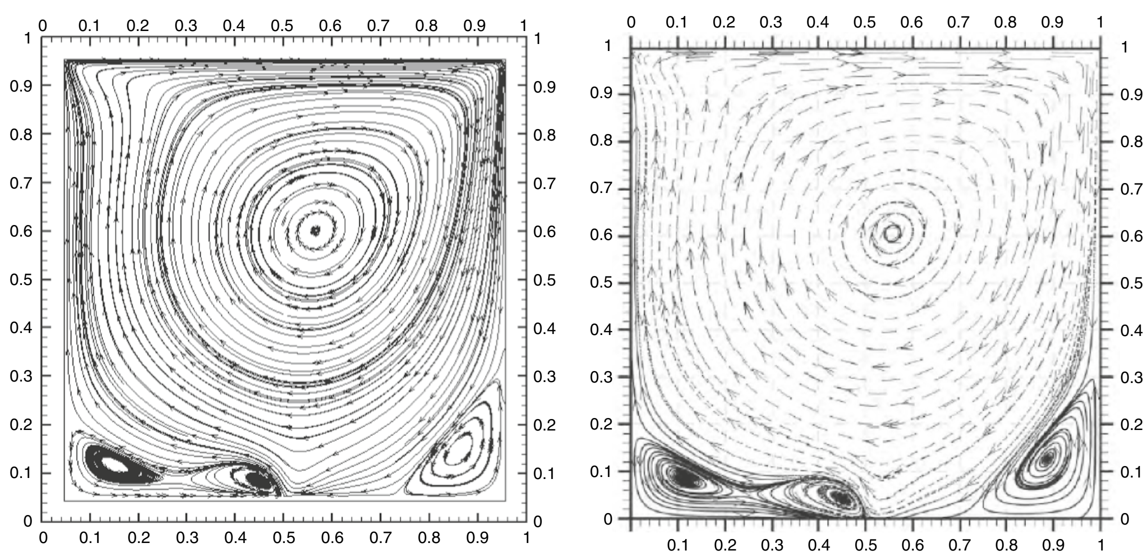

(a) Present simulation results

(b) Tzirtzilakis and Xenos study [95]

Fig. 3 Comparison of streamlines in a cavity due to FHD with [95]

Geometry definition and boundary conditions

In the current article, a wavy duct as shown in Fig. 1 is studied. The direction of the fluid flow is in wave form with a sine curve expressed by the trigonometric function, as below.

$$y = A \sin\left(2\pi \cdot \frac{z}{\lambda}\right) \tag{19}$$

where A and k are defined as amplitude and wavelength, respectively. The SIMPLE velocity–pressure coupling method is used for simulation. To discretize the convection terms, second-order upwind scheme is employed. The results of mesh independency examination are shown in Fig. 1c. Two maximum grids are in good agreement with each other in value of average Nusselt, and their tolerance is lower than 1%; therefore, a grid with 1,700,000 elements is selected and used for this simulation (Fig. 2).

Simulation, geometry and boundary conditions data are presented in Table 1.

Table 2 Simulation condition for magnetic field effect

R_e	h /μm	Mn	%V.F	T_{in}/K
200	25	0	4	298.15
200	25	1,300,000	4	298.15
200	25	2,000,000	4	298.15
200	25	3,000,000	4	298.15
200	25	4,000,000	4	298.15
200	25	5,000,000	4	298.15
200	25	8,000,000	4	298.15

For validation a comparison between the theoretical investigation and present simulation is shown in Fig. 3. It can be observed that the current outputs are in excellent agreement with theoretical one. For the magnetic field validation, the velocity profile of fluid flow imposed by an external magnetic field in a channel which is done by Aminifar et al. [94] is considered. The results predicted a good agreement between results in this study and Aminifar et al. study.

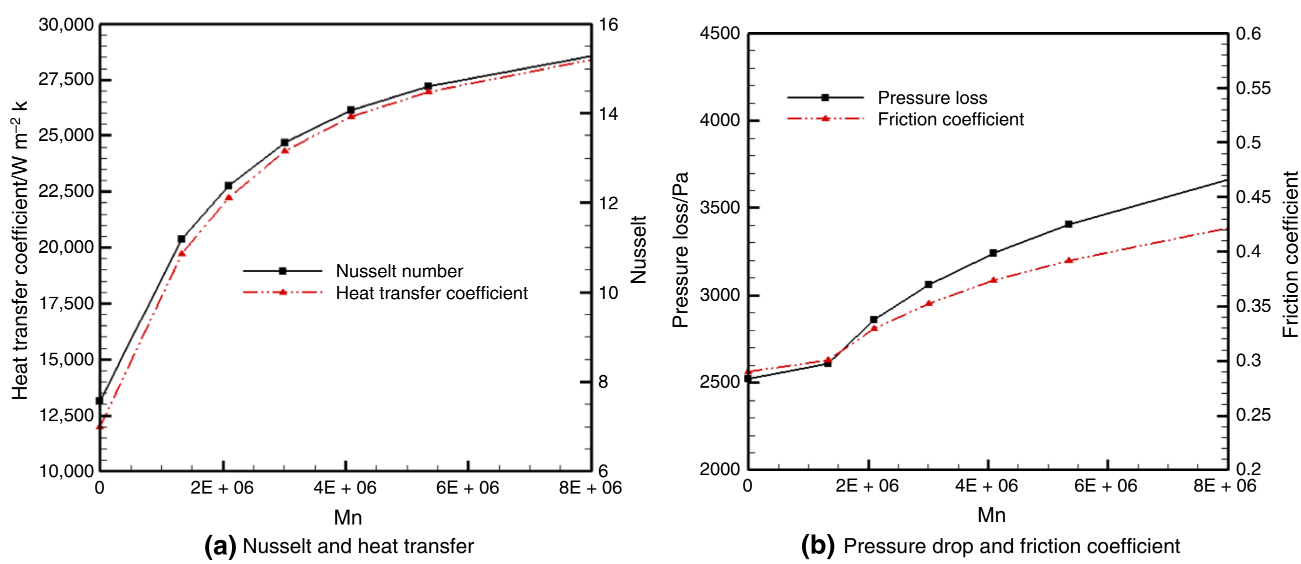

Fig. 4 Effect of magnetic number on thermophysical parameters

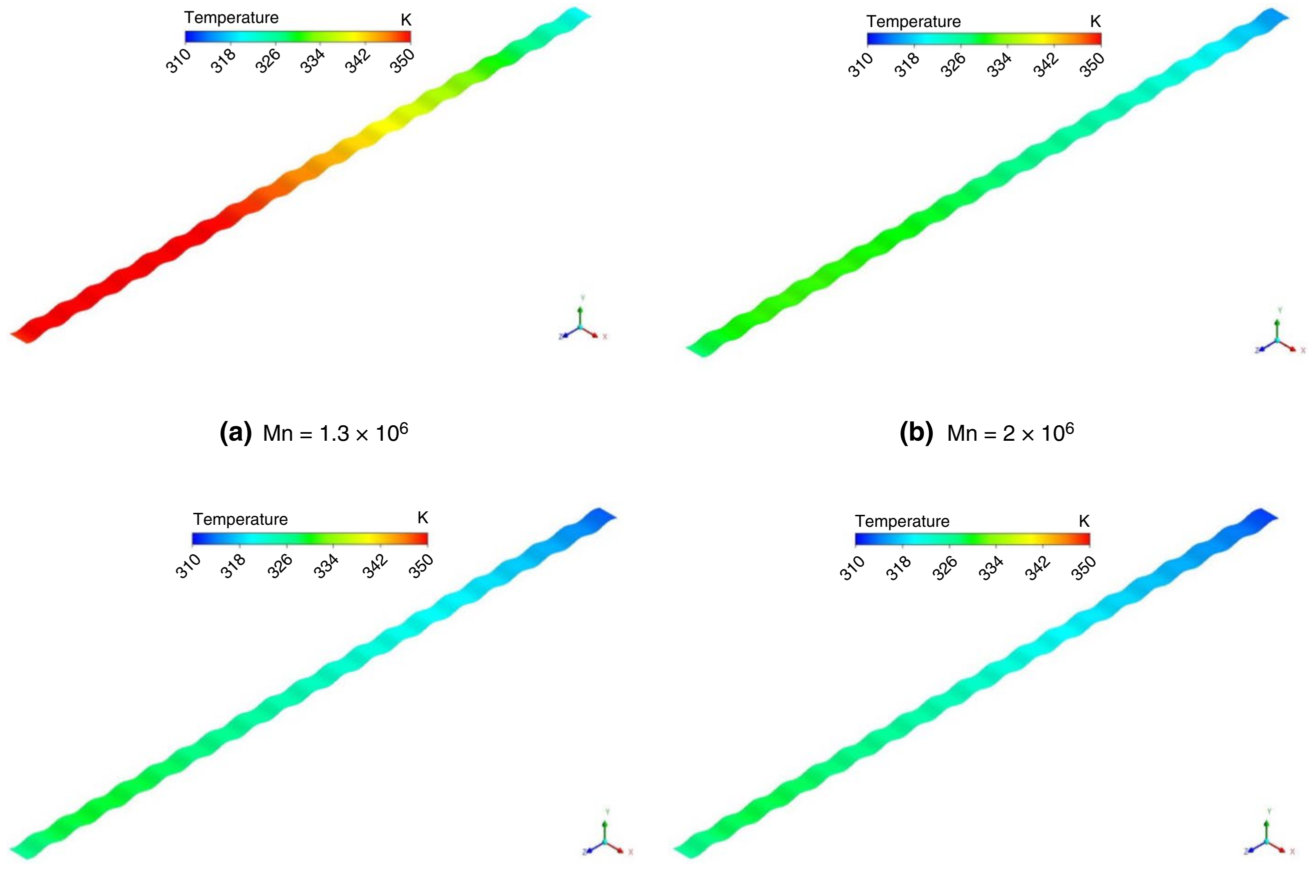

(a) Mn = 1.3×10^6 **(b)** Mn = 2×10^6

(c) Mn = 5×10^6 **(d)** Mn = 8×10^6

Fig. 5 Effect of magnetic number on bottom wall temperature

Furthermore, the streamlines due to the external magnetic field under a channel in our simulation are compared with Tzirtzilakis and Xenosstudy [95] at $R_e = 400$ and Mn = 256 (Fig. 4). There is a proper and very good treaty between results of current code and [95].

Results

In this section the effect of different influential parameters is studied. To better consideration and assessment of parameters effect, in every section one parameter is considered as variable and the rest of them are considered fixed. Figure 4 illustrates the impact of *B* on thermophysical parameters (see Table 2).

As it is obvious by augmenting Mn due to the increasing recirculation and fluid–solid interaction, the thermal boundary layer has been affected and consequently the Nusselt number and heat transfer are increased. Furthermore, it is clear that due to the increase in fluid–solid interaction, the pressure loss and friction coefficient are enhanced.

Figure 5 shows a comparison of the wall temperature in various magnetic numbers. As it can be seen, by increasing

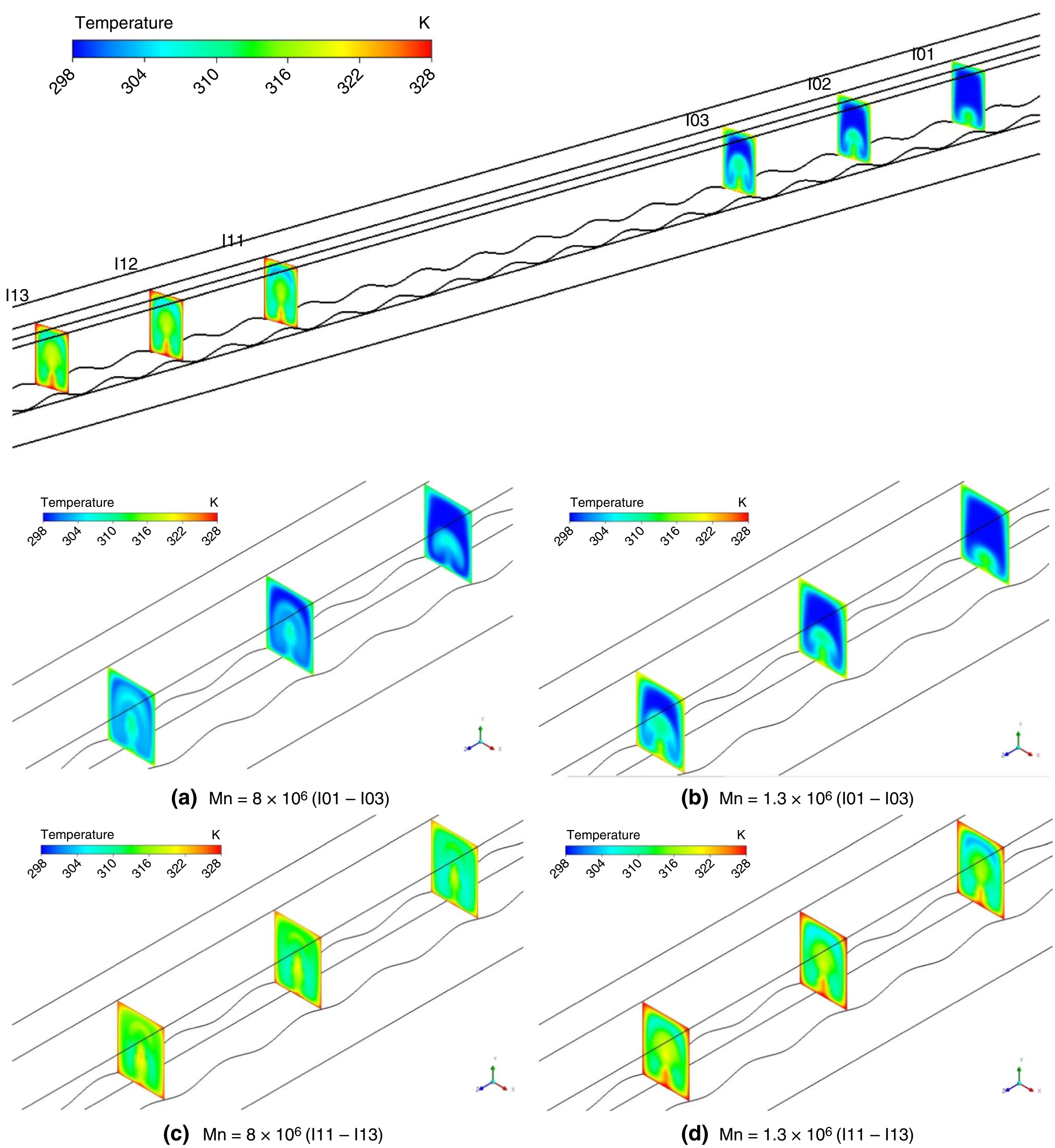

Fig. 6 Effect of magnetic number on temperature distribution in nanofluid

Table 3 Simulation condition for volume fraction effect

R_e	h/μm	Mn	%V.F	Tin/K
200	25	2,000,000	0.5	298.15
200	25	2,000,000	1	298.15
200	25	2,000,000	2	298.15
200	25	2,000,000	4	298.15

the magnetic number because of increasing the wall–fluid interaction and collision, and as a result increasing the heat transfer rate, the temperature of the bottom wall is significantly decreased and it shows the significant impact of Mn on cooling application in microchannels.

Figure 6 presents a comparison between nanofluid temperatures in different cross sections in the microchannel

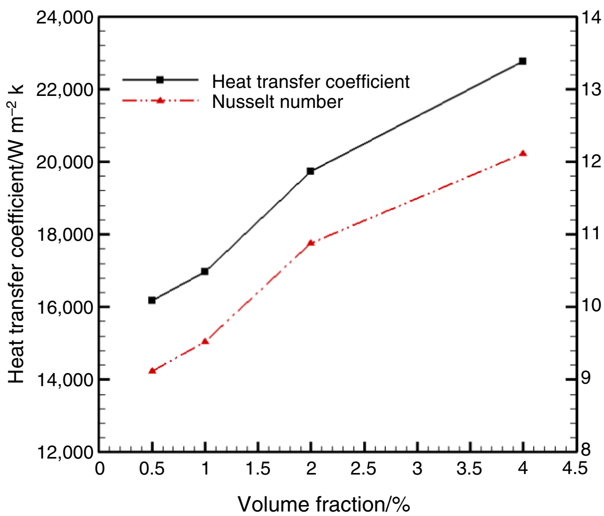

(a) Nusselt number and heat transfer coefficient

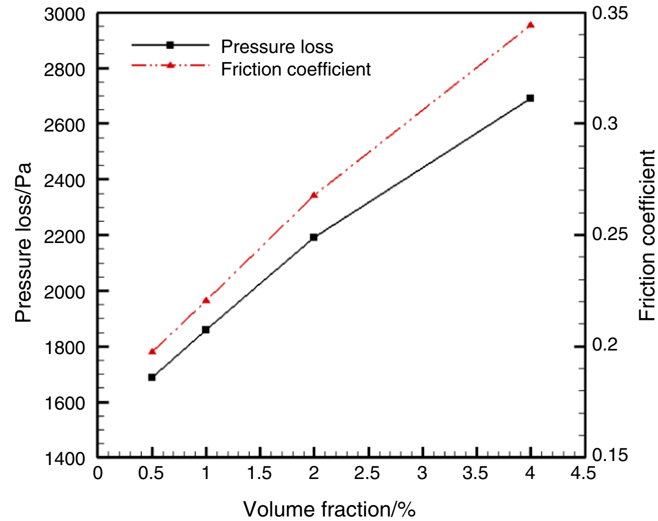

(b) Friction coefficient and pressure drop

Fig. 7 The effect of volume fraction on thermophysical properties

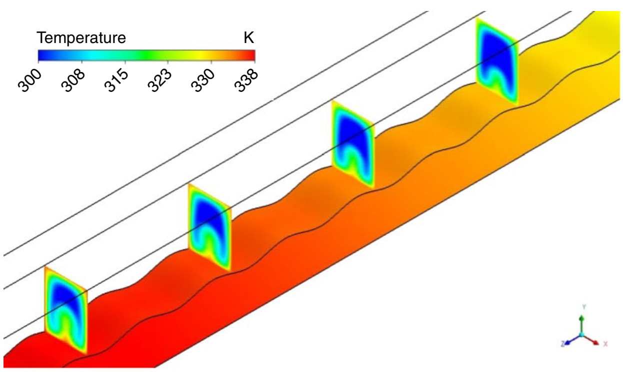

(a) 0.5% Vf

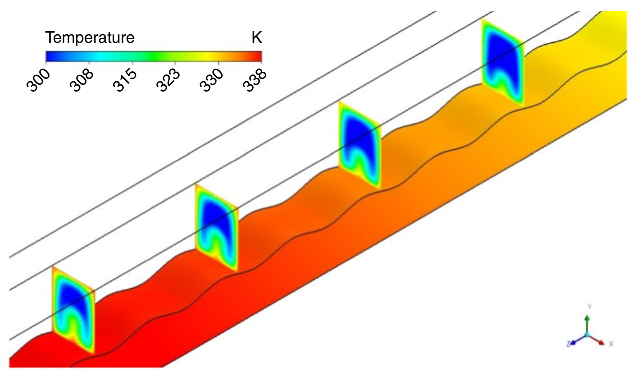

(b) 1% Vf

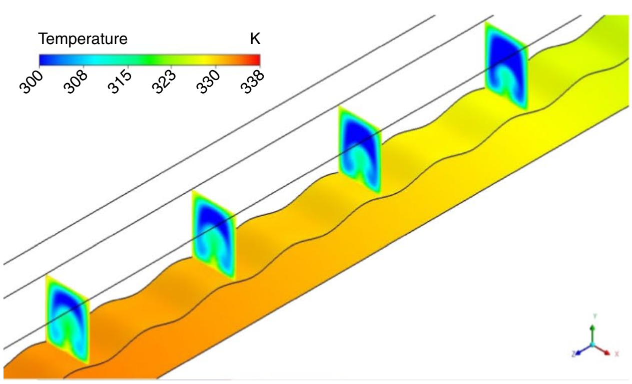

(c) 2% Vf

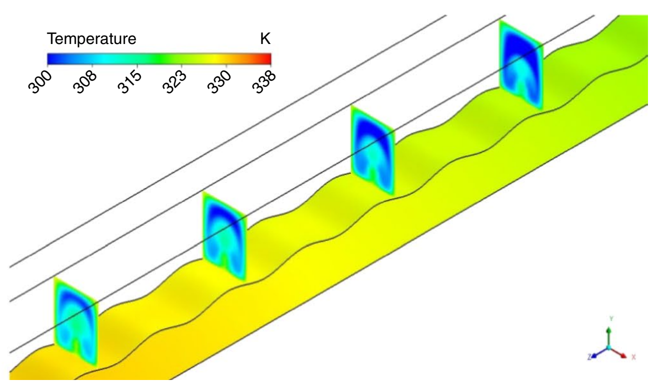

(d) 4% Vf

Fig. 8 Temperature distribution for various volume fraction

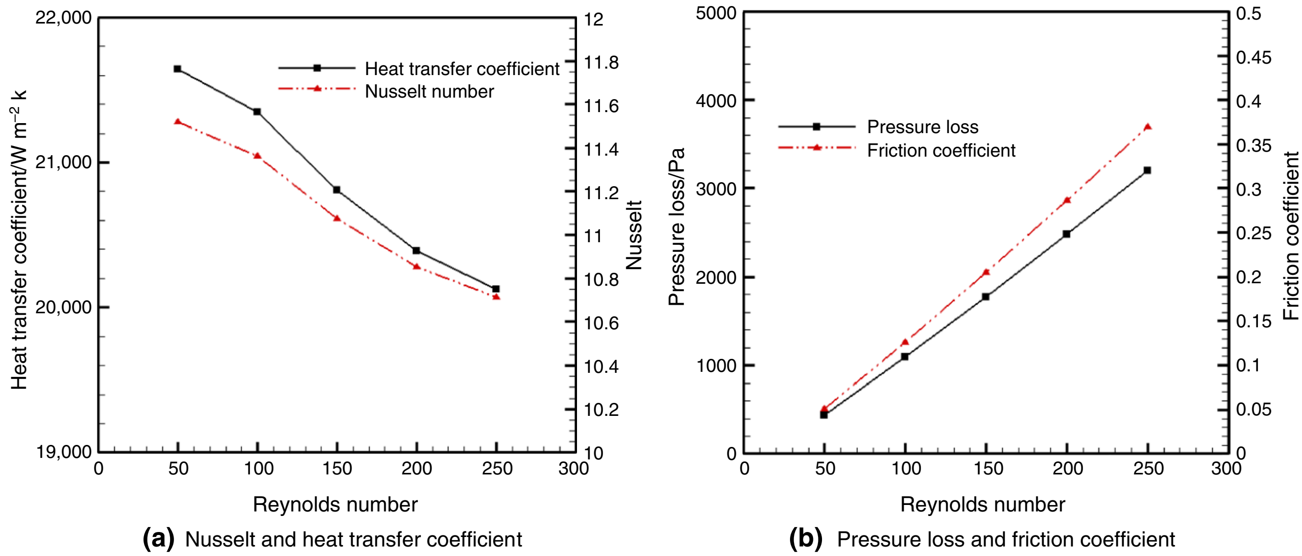

Fig. 9 Effect of Reynolds number on thermophysical parameters

Table 4 Simulation condition for Reynolds number effect

h/μm	Mn	%V.F	T_{in}/K
25	1,300,000	4	298.15
25	1,300,000	4	298.15
25	1,300,000	4	298.15
25	1,300,000	4	298.15
25	1,300,000	4	298.15

under influence of different magnitudes of magnetic field. It is clear that, from the inlet toward the outlet, the temperature of the ferrofluid due to the heat transfer between hot wall and nanofluid is increased; however, it is demonstrated that by increasing the magnetic number, because of increasing recirculation in fluid and increasing collision, the diffusivity of heat transfer in the fluid is increased and the maximum temperature in the outlet flow for the higher magnetic number is lower and also the temperature distribution is more uniform in the fluid field.

The impact of volume fraction of magnetic nanoparticles is investigated in Fig. 5 and Table 3.

It is shown that by increasing the volume fraction, the heat transfer coefficient and Nusselt number that are representative of heat transfer augmentation are enhanced. The results indicate that by augmenting the φ from 0.5 to 4.5%, the Nusselt number is increased by 33.3%. It is due to the increase in the wall–fluid interaction because of increasing the magnetic field effect on flow field by increasing the volume fraction. Friction coefficient and pressure loss are also increased by augmenting φ, about 0.63% and 0.66%, respectively (Fig. 7).

Effect of volume fraction on temperature distribution on the nanofluid field and microchannel wall is presented in Fig. 8. It is conducted that by augmenting φ, as it is mentioned, due to the increasing magnetic field effect and consequently fluid–solid interaction, the temperature on the wall along the channel is decreased. The diffusivity of heat transfer on the fluid by increasing volume fraction is also increased, and the temperature distribution is changed in the flow field (Fig. 9).

Reynolds number is another physical parameter that has been investigated in this study (see Table 4).

The results illustrated that in a constant magnetic field, increasing the Reynolds number has an opposite effect on Nusselt and also heat transfer coefficient. By increasing the Reynolds from 50 to 250, the Nusselt and heat transfer decreased by about 8.6%. Increasing Reynolds number reduces the hydrodynamics and thermal boundary layer and consequently the heat transfer coefficient. However, in this investigation, the results demonstrated that magnetic

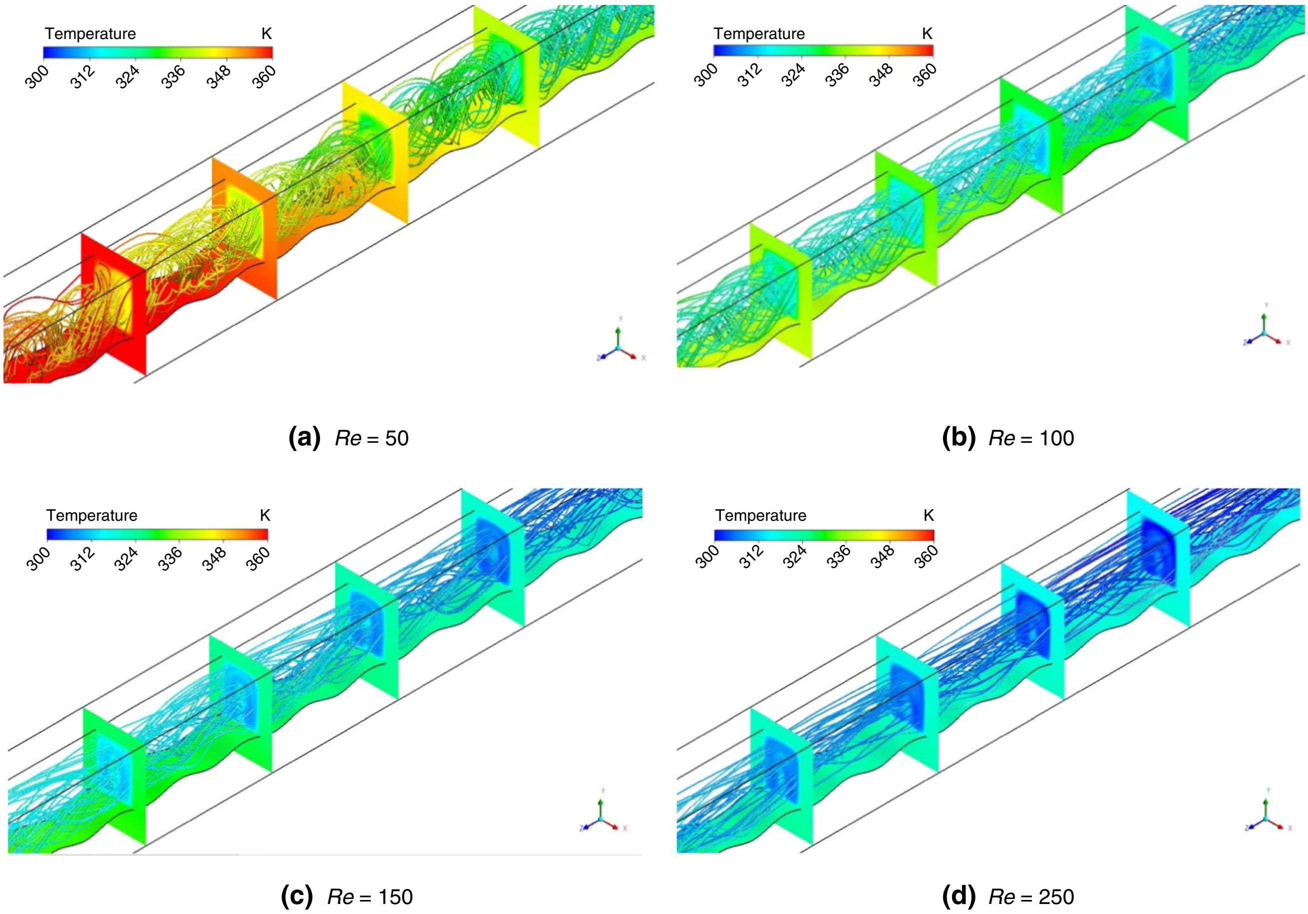

Fig. 10 Temperature distribution and streamlines for various Reynolds number

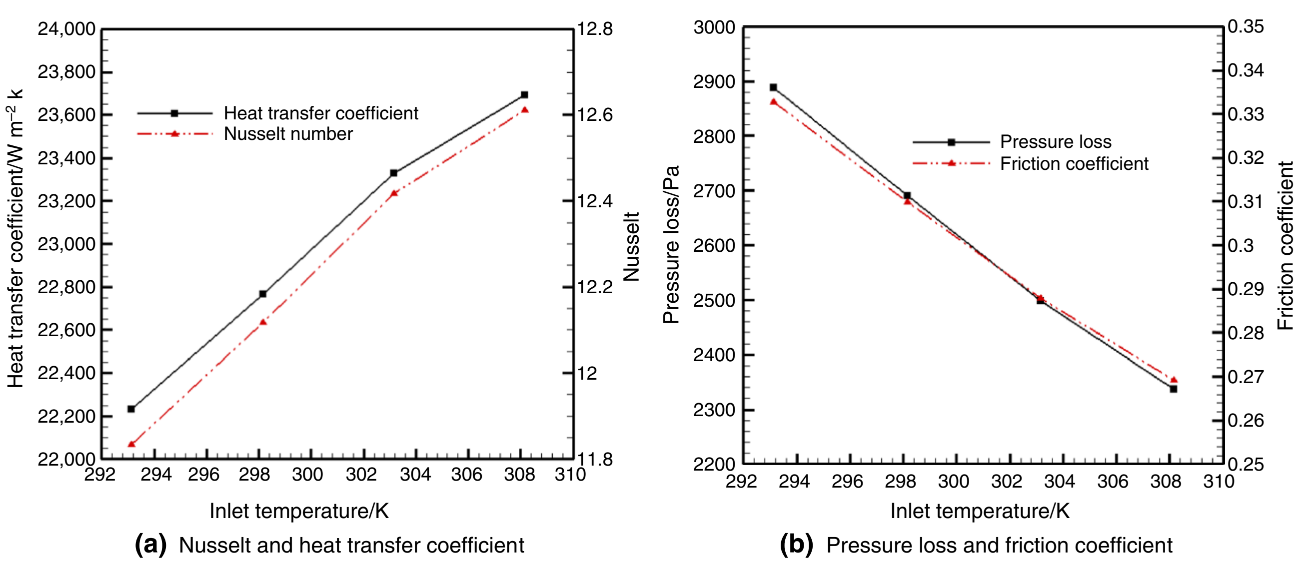

Fig. 11 Effect of inlet temperature on thermophysical properties

Table 5 Simulation condition for inlet temperature effect

R_e	h/μm	Mn	%V.F	T_{in}/K
200	25	2,000,000	4	293.15
200	25	2,000,000	4	298.15
200	25	2,000,000	4	303.15
200	25	2,000,000	4	308.15

Table 6 Simulation condition for wave's amplitude effect

R_e	h/μm	Mn	%V.F	T_{in}/K
200	0	1,300,000	4	298.15
200	25	1,300,000	4	298.15
200	50	1,300,000	4	298.15
200	100	1,300,000	4	298.15

number has a more dominant effect and compares the Reynolds number effect. Consequently, when the Reynolds number increases, the impact of Mn will reduce and also the total effect leads to a decrease in heat transfer. Additionally, it is revealed that augmenting the Reynolds number will rise the friction coefficient and pressure drop significantly by about 6 and 8 times, respectively.

Figure 10 shows a comparison of temperature contour and streamlines for various Reynolds numbers. As it is clear from the figure, in the lowest Reynolds number due to the higher amount of magnetic field effect on nanofluid compared to the inertia force, the flow field experienced higher intensity of recirculation and consequently interaction with walls. Therefore, heat transfer between hot wall and cold nanofluid is increased, and as it is obvious, the fluid temperature is much higher than other cases in the domain. However, by increasing Reynolds number, because of increasing the momentum of the fluid and consequently inertia force, the influence of magnetic field is faded. By decreasing the effect of magnetic field, the intensity of recirculation and interaction between fluid and wall are decreased, and as a result, the diffusivity of heat on the fluid is reduced and the fluid temperature is decreased.

Figure 11 illustrates the impact of inlet temperature on thermophysical properties.

It is cleared that by increasing inlet temperature, due to reducing the viscosity the pressure drop and friction

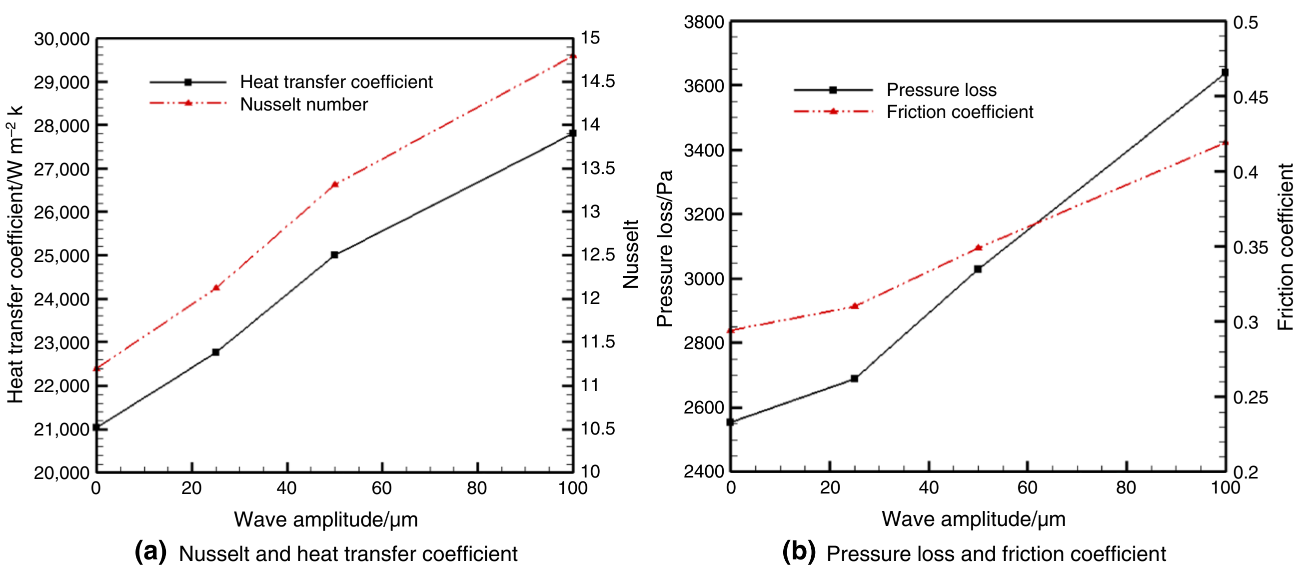

Fig. 12 Effect of wave amplitude on thermophysical properties

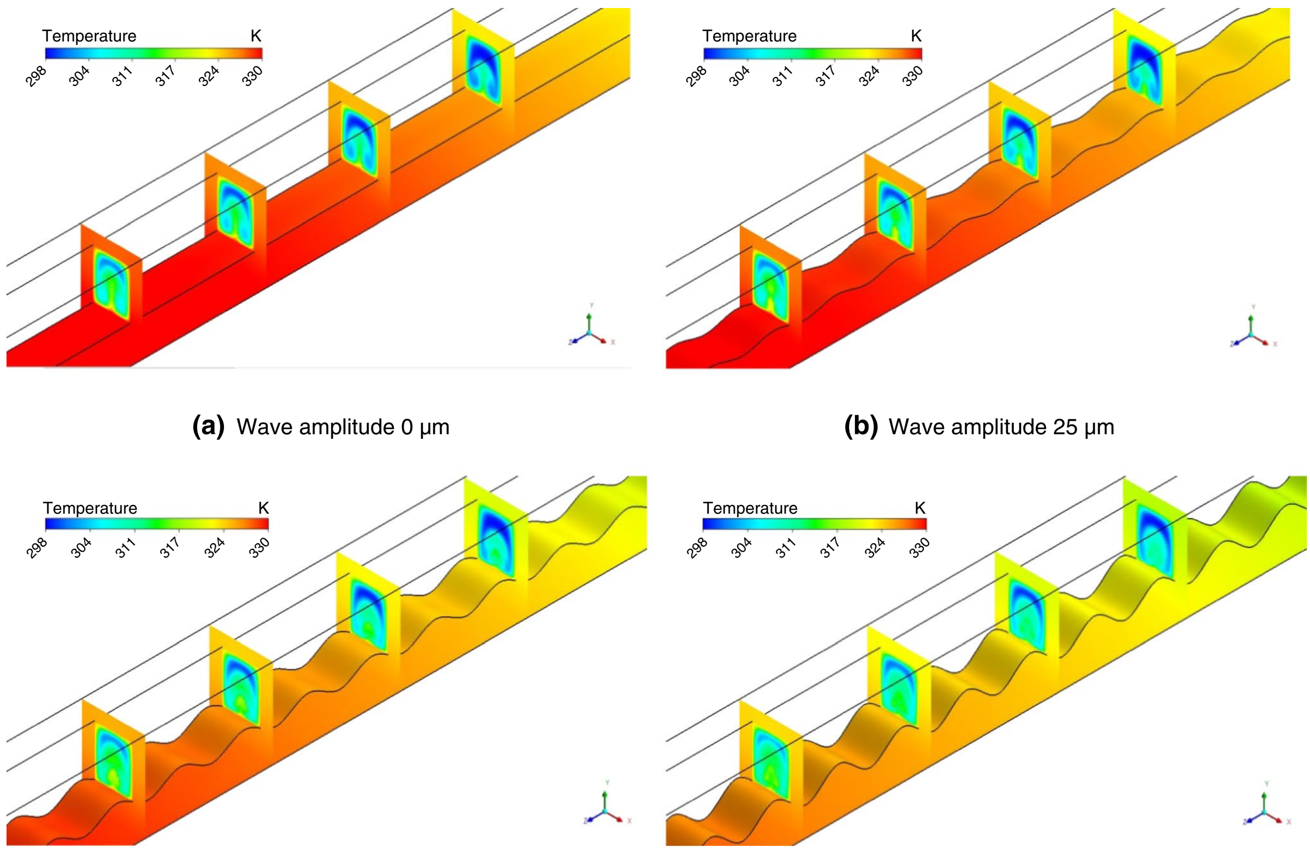

(a) Wave amplitude 0 μm

(b) Wave amplitude 25 μm

(c) Wave amplitude 50 μm

(d) Wave amplitude 75 μm

Fig. 13 Temperature distribution in various amplitudes of wavy wall

coefficient are reduced (see Table 5). However, inlet temperature compared to other considered parameters did not have a significant effect on thermal performance and there is a just slight increase in both Nusselt and heat transfer coefficient. Another parameter that is investigated in wavy microchannel in presence of external magnetic field is wave's amplitude (see Table 6).

It is revealed that by increasing wave amplitude, due to the increase in the recirculation size and intensity, the interaction of fluid and structure is increased and consequently a noteworthy augmentation in the Nu by about 40%, respectively, has been observed. On the other hand, increasing fluid–solid collision increased the friction coefficient and pressure drop significantly that is a negative effect in channels (Fig. 12).

Temperature distribution in various amplitudes of wavy wall is shown in Fig. 13. It is illustrated that by increasing the amplitude, due to the increase in the interaction momentum and recirculation, the heat diffusivity on the ferrofluid is increased, and consequently, the temperature on the surface decreased along the channel and the fluid experienced more uniform temperature and more average temperature in higher amplitudes.

As it is mentioned in the paper, for this study the viscosity of fluid is considered as a multivariable dependence variables consisted of temperature, volume fraction

Fig. 14 Influence of various parameters on viscosity distribution

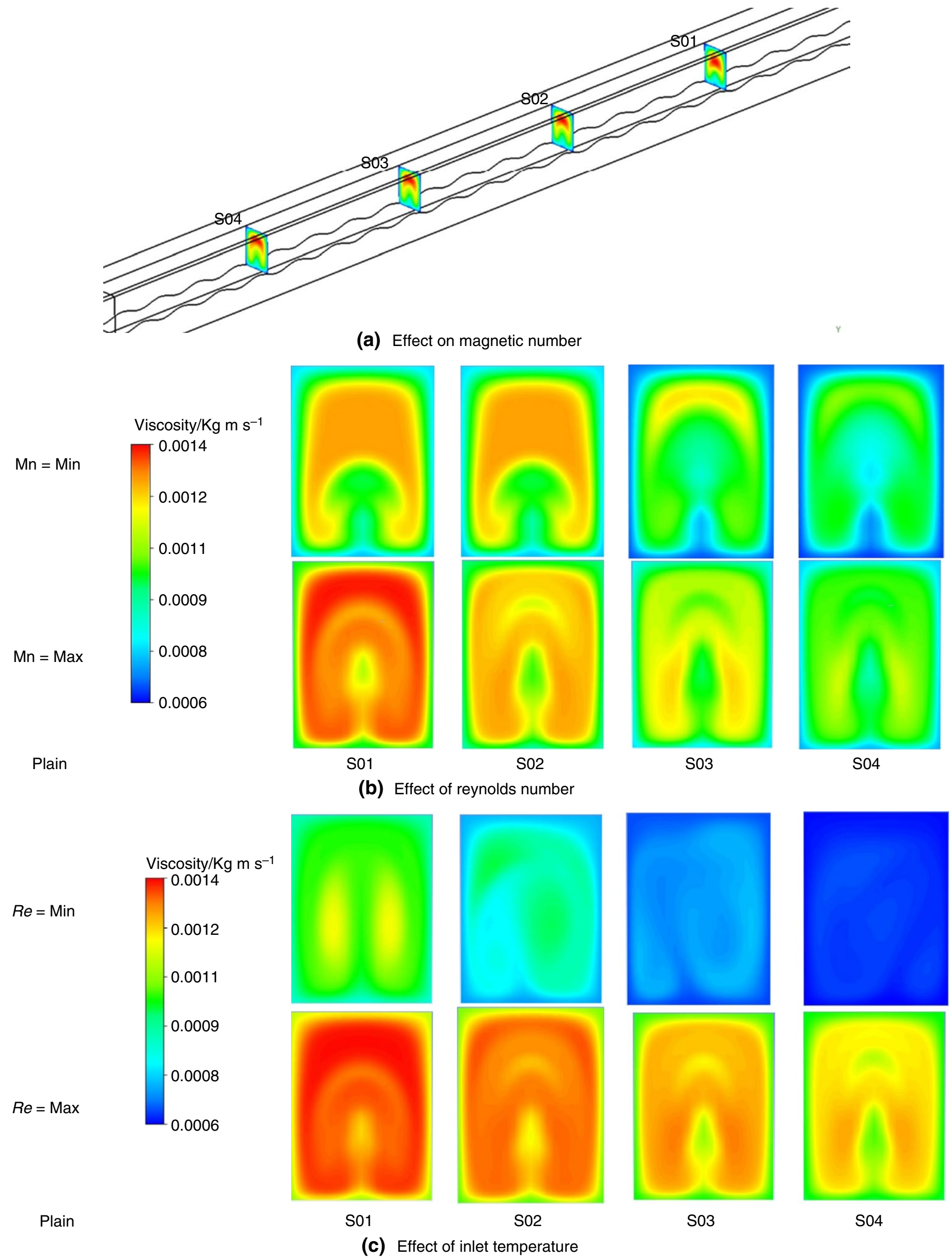

and magnetic field magnitude; therefore, in this section the changes on viscosity distribution in the ferrofluid are investigated. For this purpose, the temperature contour of four cross sections along the microchannel is considered. The results show that by increasing magnetic number the viscosity of fluid is increased and also a more uniform distribution of viscosity can be observed in the case with the highest magnetic number. The changes of the viscosity by Reynolds number show that in the higher Reynolds number due to the lower temperature, the viscosity is reduced in the ferrofluid. Comparison of the effect of inlet temperature on viscosity indicates that in the minimum

Fig. 14 (continued)

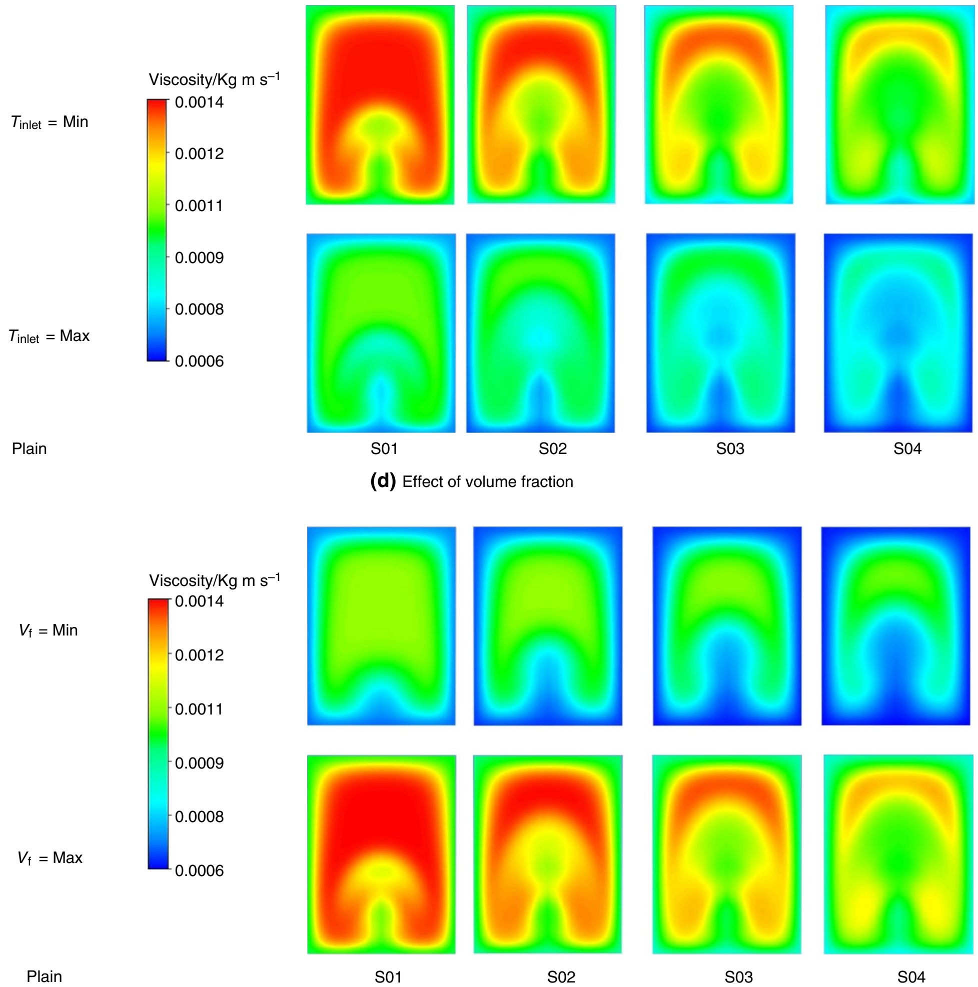

studied inlet temperature, due to the minimum temperature of ferrofluid in the domain, the viscosity is lower than higher inlet temperature and maximum one. Additionally, it is illustrated by augmenting the φ of ferrofluid, and the viscosity in the domain is increased. In all the figures, it can be observed that the overall viscosity range in the domain alongside the microchannel from inlet to outlet is increased and it is because of enhancing temperature of the fluid field from inlet to outlet (Fig. 14).

Comparison for different investigated parameters on friction coefficient and Nu is illustrated in Fig. 15. As it is clear from the figure, excepted of Reynolds number in constant magnetic field, the rest of considered variables showed a positive effect on Nusselt number; meanwhile, the magnetic field and wave amplitude have the most influence, respectively. Also it is conducted although the amount of the friction coefficient for the wave amplitude and magnetic number is more than other variables and points because of the Reynolds number in which their effect studied on in (maximum $R_e = 250$), however, depends on the trend of the graphs, and increase in Reynolds number is shown the worst effect on friction coefficient and consequently pressure loss.

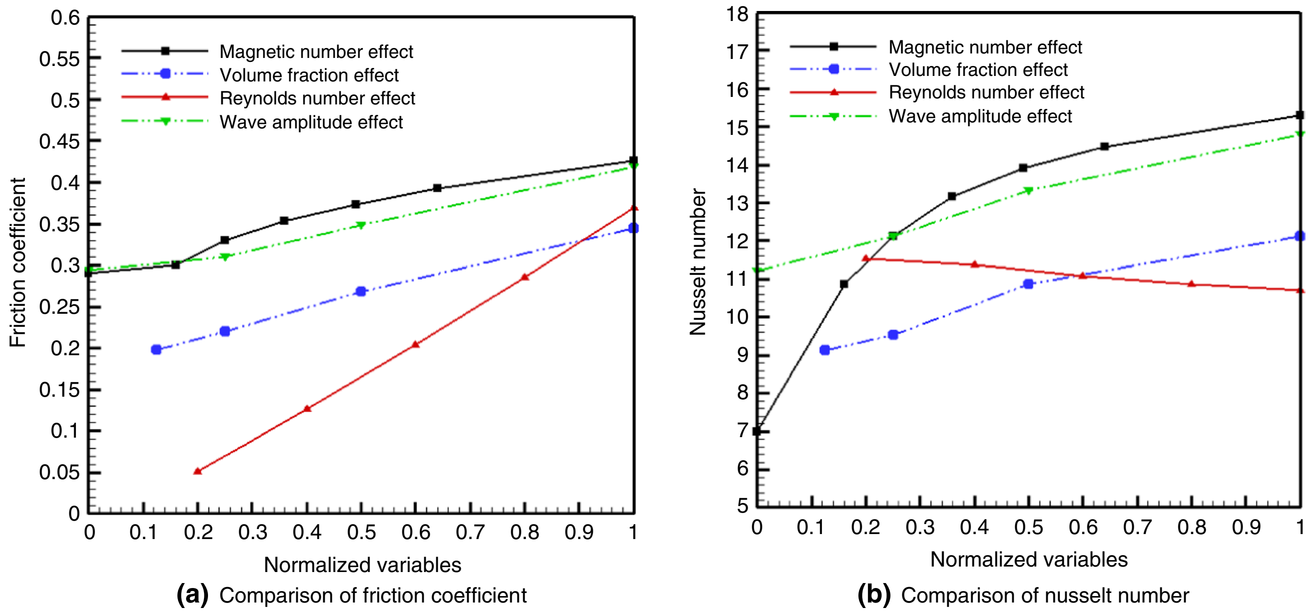

Fig. 15 Comparison of influence of parameters on friction coefficient and Nusselt number as non-dimensional variables

Conclusions

Treatment of a ferrofluid with a multivariable dependence viscosity in a microchannel under impact of an external non-uniform magnetic field due to a current-carrying wire is studied. The effect of various variables such as inlet temperature, R_e, magnetic field magnitude and volume fraction on Nu, heat transfer coefficient, friction coefficient and pressure loss. The simulation conditions of all investigated cases are explained in results section. The results predicted that the magnetic field intensity growing has a important role on heat transfer augmentation and improving heat transfer and cooling in the microchannel; however, due to the increasing collision and interaction between ferrofluid and structure, the friction coefficient and pressure loss are also increased. Reynolds number showed a significant influence on increasing friction effect and pressure loss; however, in the lower Reynolds number, magnetic effect showed a more dominant effect compared to Reynolds and augmenting Nu. In the higher volume fraction the influence of Kelvin force is higher than lower magnetic number, and therefore due to the increasing recirculation and fluid–solid interaction, the Nu increased. Investigation of viscosity distribution in the fluid domain showed a significant change due to the magnetic field and volume fraction. A comparison among variables effect as non-dimensional parameters showed that Reynolds number and volume fraction had a worst effect on friction coefficient, whereas magnetic number and wave's amplitude increasing had a best impact on heat transfer augmentation.

References

1. Hajatzadeh Pordanjani A, Aghakhani S, Afrand M, Mahmoudi B, Mahian O, Wongwises S. An updated review on application of nanofluids in heat exchangers for saving energy. Energy Convers Manag. 2019;198:111886.
2. Szilágyi IM, Kállay-Menyhárd A, Šulcová P, Kristóf J, Pielichowski K, Šimon P. Recent advances in thermal analysis and calorimetry presented at the 1st Journal of Thermal Analysis and Calorimetry Conference and 6th V4 (Joint Czech-Hungarian-Polish-Slovakian) Thermoanalytical Conference (2017). J Therm Anal Calorim. 2018;133(1):1–4.
3. Sheikholeslami M. New computational approach for exergy and entropy analysis of nanofluid under the impact of Lorentz force through a porous media. Comput Methods Appl Mech Eng. 2019;344:319–33.
4. Sheikholeslami M, Haq R, Shafee A, Li Z. Heat transfer behavior of Nanoparticle enhanced PCM solidification through an enclosure with V shaped fins. Int J Heat Mass Transf. 2019;130:1322–42.
5. Nikkhah V, Sarafraz MM, Hormozi F, Peyghambarzadeh SM. Particulate fouling of CuO–water nanofluid at isothermal diffusive condition inside the conventional heat exchanger-experimental and modeling. Exp Thermal Fluid Sci. 2015;60:83–95.
6. Sheikholeslami M, Zeeshan A. Analysis of flow and heat transfer in water based nanofluid due to magnetic field in a porous enclosure with constant heat flux using CVFEM. Comput Methods Appl Mech Eng. 2017;320:68–81.
7. Sheikholeslami M, Arabkoohsar A, Shafee A, Ismail KAR. Second law analysis of a porous structured enclosure with nano-enhanced phase change material and under magnetic force. J Thermal Anal Calorim. 2020. https://doi.org/10.1007/s10973-019-08979-y.
8. Sheikholeslami M, Rezaeianjouybari B, Shafee A, Li Z, Nguyen TK. Application of nano-refrigerant for boiling heat transfer enhancement employing an experimental study. Int J Heat Mass Transf. 2019;141:974–80.

9. Sheikholeslami M, Sadoughi MK. Simulation of CuO–water nanofluid heat transfer enhancement in presence of melting surface. Int J Heat Mass Transf. 2018;116:909–19.
10. Sheikholeslami M, Jafaryar M, Hedayat M, Shafee A, Li Z, Nguyen TK, Bakouri M. Heat transfer and turbulent simulation of nanomaterial due to compound turbulator including irreversibility analysis. Int J Heat Mass Transf. 2019;137:1290–300.
11. Sheikholeslami M, Shehzad SA. CVFEM for influence of external magnetic source on $Fe_3O4–H_2O$ nanofluid behavior in a permeable cavity considering shape effect. Int J Heat Mass Transf. 2017;115:180–91.
12. Sheikholeslami M, Barzegar Gerdroodbary M, Shafee A, Tlili I (2019) Hybrid nanoparticles dispersion into water inside a porous wavy tank involving magnetic force. J Thermal Anal Calorim. 2019. https://doi.org/10.1007/s10973-019-08858-6.
13. Sheikholeslami M, Jafaryar M, Shafee A, Li Z, Haq R. Heat transfer of nanoparticles employing innovative turbulator considering entropy generation. Int J Heat Mass Transf. 2019;136:1233–40.
14. Sheikholeslami M, Haq R, Shafee A, Li Z, Elaraki YG, Tlili I. Heat transfer simulation of heat storage unit with nanoparticles and fins through a heat exchanger. Int J Heat Mass Transf. 2019;135:470–8.
15. Ma X, Sheikholeslami M, Jafaryar M, Shafee A, Nguyen-Thoi T, Li Z. Solidification inside a clean energy storage unit utilizing phase change material with copper oxide nanoparticles. J Cleaner Prod. 2020;245:118888. https://doi.org/10.1016/j.jclepro.2019.118888.
16. Sheikholeslami M, Arabkoohsar A, Jafaryar M. Impact of a helical-twisting device on nanofluid thermal hydraulic performance of a tube. J Therm Anal Calorim. 2019. https://doi.org/10.1007/s10973-019-08683-x.
17. Seyednezhad M, Sheikholeslami M, Ali JA, Shafee A, Nguyen TK. Nanoparticles for water desalination in solar heat exchanger, Review. J Thermal Anal Calorim. 2019. https://doi.org/10.1007/s10973-019-08634-6.
18. Sheikholeslami M, Shehzad SA, Li Z, Shafee A. Numerical modeling for alumina nanofluid magnetohydrodynamic convective heat transfer in a permeable medium using Darcy law. Int J Heat Mass Transf. 2018;127:614–22.
19. Sheikholeslami M, Shehzad SA. Numerical analysis of Fe_3O_4–H_2O nanofluid flow in permeable media under the effect of external magnetic source. Int J Heat Mass Transf. 2018;118:182–92.
20. Sheikholeslami M, Li Z, Shafee A. Lorentz forces effect on NEPCM heat transfer during solidification in a porous energy storage system. Int J Heat Mass Transf. 2018;127:665–74.
21. Szilágyi IM, Santala E, Heikkilä M, Kemell M, Nikitin T, Khriachtchev L, Räsänen M, Ritala M, Leskelä M. Thermal study on electrospun polyvinylpyrrolidone/ammonium metatungstate nanofibers: optimising the annealing conditions for obtaining WO3 nanofibers. J Therm Anal Calorim. 2011;105(1):73.
22. Sheikholeslami M. Influence of Coulomb forces on Fe3O4-H2O nanofluid thermal improvement. Int J Hydrogen Energy. 2017;42:821–9.
23. Sheikholeslami Mohsen. Lattice Boltzmann method simulation of MHD non-Darcy nanofluid free convection. Phys B. 2017;516:55–71.
24. Sheikholeslami M, Darzi M, Li Z. Experimental investigation for entropy generation and exergy loss of nano-refrigerant condensation process. Int J Heat Mass Transf. 2018;125:1087–95.
25. Sheikholeslami M. Numerical approach for MHD Al_2O_3-water nanofluid transportation inside a permeable medium using innovative computer method. Comput Methods Appl Mech Eng. 2019;344:306–18.
26. Rosa AP, Cunha FR. The influence of dipolar particle interactions on the magnetization and the rotational viscosity of ferrofluids. Phys Fluids. 2019;31:052006.
27. Sheikholeslami M, Jafaryar M, Saleem S, Li Z, Shafee A, Jiang Y. Nanofluid heat transfer augmentation and exergy loss inside a pipe equipped with innovative turbulators. Int J Heat Mass Transf. 2018;126:156–63.
28. Qin Y. Urban canyon albedo and its implication on the use of reflective cool pavements. Energy Build. 2015;96:86–94.
29. Sheikholeslami M, Ghasemi A, Li Z, Shafee A, Saleem S. Influence of CuO nanoparticles on heat transfer behavior of PCM in solidification process considering radiative source term. Int J Heat Mass Transf. 2018;126:1252–64.
30. Sheikholeslami M, Shehzad SA, Li Z. Water based nanofluid free convection heat transfer in a three dimensional porous cavity with hot sphere obstacle in existence of Lorenz forces. Int J Heat Mass Transf. 2018;125:375–86.
31. Li Z, Li D, Cui H, Zhang Y, Wang H. Influence of the carrier fluid viscosity on the rotational and oscillatory rheological properties of ferrofluids. J Nanosci Nanotechnol. 2019;19:5572–81.
32. Rostamian H, Lotfollahi MN. A novel statistical approach for prediction of thermal conductivity of CO_2 by response surface methodology. Physica A. 2019;527:121175.
33. Sheikholeslami M, Jafaryar M, Li Z. Nanofluid turbulent convective flow in a circular duct with helical turbulators considering CuO nanoparticles. Int J Heat Mass Transf. 2018;124:980–9.
34. Sheikholeslami M, Ghasemi A. Solidification heat transfer of nanofluid in existence of thermal radiation by means of FEM. Int J Heat Mass Transf. 2018;123:418–31.
35. Sheikholeslami M, Mahian O. Enhancement of PCM solidification using inorganic nanoparticles and an external magnetic field with application in energy storage systems. J Clean Prod. 2019;215:963–77.
36. Sheikholeslami M, Rokni HB. Numerical modeling of nanofluid natural convection in a semi annulus in existence of Lorentz force. Comput Methods Appl Mech Eng. 2017;317:419–30.
37. Sheikholeslami M, Shehzad SA. CVFEM simulation for nanofluid migration in a porous medium using Darcy model. Int J Heat Mass Transf. 2018;122:1264–71.
38. Sheikholeslami M, Darzi M, Sadoughi MK. Heat transfer improvement and pressure drop during condensation of refrigerant-based Nanofluid. An experimental procedure. Int J Heat Mass Transf. 2018;122:643–50.
39. Taslimifar M, Mohammadi M, Afshin H, Saidi MH. Overall thermal performance of ferro fluidic open loop pulsating heat pipes: an experimental approach. Int J Therm Sci. 2013;65:234–41.
40. Gandomkar A, Saidi MH, Shafii MB, Vandadi M, Kalan K. Visualization and comparative investigations of pulsating ferrofluid heat pipe. Appl Thermal Eng. 2017;116:56–65.
41. Khoshmehr HH, Saboonchi A, Shafii MB, Jahani N. The study of magnetic field implementation on cylinder quenched in boiling ferro-fluid. Appl Therm Eng. 2014;64:331–8.
42. Ahmad B, Iqbal Z. Framing the performance of variation in resistance on viscous dissipative transport of ferro fluid with homogeneous and heterogeneous reactions. J Mol Liq. 2017;241:904–11.
43. Strek T, Jopek H. Computer simulation of heat transfer through a ferrofluid. J Solid State Phys. 2006;244:1027–37.
44. Shima A, Philip PD. Tuning of thermal conductivity and rheology of nanofluids using an external stimulus. J Phys Chem C. 2011;115:20097–104.
45. Rabbi KM, Sheikholeslami M, Karim A, Shafee A, Li Z, Tlili I. Prediction of MHD flow and entropy generation by artificial neural network in square cavity with heater-sink for nanomaterial. Physica A Stat Mech Appl Physica A. 2020;541:123520.

46. Sheikholeslami M, Nematpour Keshteli A, Babazadeh H. Nanoparticles favorable effects on performance of thermal storage units. J Mol Liq, 2020. https://doi.org/10.1016/j.molliq.2019.112329.
47. Sheikholeslami M, Shehzad SA. Simulation of water based nanofluid convective flow inside a porous enclosure via Non-equilibrium model. Int J Heat Mass Transf. 2018;120:1200–12.
48. Sheikholeslami Mohsen, Seyednezhad Mohadeseh. Simulation of nanofluid flow and natural convection in a porous media under the influence of electric field using CVFEM. Int J Heat Mass Transf. 2018;120:772–81.
49. Shafee A, Sheikholeslami M, Jafaryar M, Babazadeh H, Utilizing copper oxide nanoparticles for expedition of solidification within a storage system. J Mol Liq. 2020. https://doi.org/10.1016/j.molliq.2019.112371.
50. Sheikholeslami M, Rokni HB. Numerical simulation for impact of Coulomb force on nanofluid heat transfer in a porous enclosure in presence of thermal radiation. Int J Heat Mass Transf. 2018;118:823–31.
51. Sheikholeslami M, Rokni HB. Simulation of nanofluid heat transfer in presence of magnetic field: a review. Int J Heat Mass Transfer. 2017;115:1203–33.
52. Rezaeianjouybari B, Sheikholeslami M, Shafee A, Babazadeh H, A Novel Bayesian optimization for flow condensation enhancement using nanorefrigerant: a combined analytical and experimental study. Chem Eng Sci, 2020. https://doi.org/10.1016/j.ces.2019.115465.
53. Sheikholeslami M, Hayat T, Alsaedi A. On simulation of nanofluid radiation and natural convection in an enclosure with elliptical cylinders. Int J Heat Mass Transf. 2017;115:981–91.
54. Sheikholeslami Mohsen, Rokni HB. Melting heat transfer influence on nanofluid flow inside a cavity in existence of magnetic field. Int J Heat Mass Transf. 2017;114:517–26.
55. Qin Y, Hiller JE. Understanding pavement-surface energy balance and its implications on cool pavement development. Energy Build. 2014;85:389–99.
56. Sheikholeslami M, Sadoughi M. Mesoscopic method for MHD nanofluid flow inside a porous cavity considering various shapes of nanoparticles. Int J Heat Mass Transf. 2017;113:106–14.
57. Sheikholeslami M, Bhatti MM. Forced convection of nanofluid in presence of constant magnetic field considering shape effects of nanoparticles. Int J Heat Mass Transf. 2017;111:1039–49.
58. Sheikholeslami M, Bhatti MM. Active method for nanofluid heat transfer enhancement by means of EHD. Int J Heat Mass Transf. 2017;109:115–22.
59. Sheikholeslami M. Application of Darcy law for nanofluid flow in a porous cavity under the impact of Lorentz forces. J Mol Liq. 2018;266:495–503.
60. Qin Y, Liang J, Yang H, Deng Z. Gas permeability of pervious concrete and its implications on the application of pervious pavements. Measurement. 2016;78:104–10.
61. Sheikholeslami M. Numerical modeling of Nano enhanced PCM solidification in an enclosure with metallic fin. J Mol Liq. 2018;259:424–38.
62. Sheikholeslami M. Finite element method for PCM solidification in existence of CuO nanoparticles. J Mol Liq. 2018;265:347–55.
63. Sheikholeslami Mohsen. Numerical simulation for solidification in a LHTESS by means of Nano-enhanced PCM. J Taiwan Inst Chem Eng. 2018;86:25–41.
64. Qin Y, Zhang M, Mei G. A new simplified method for measuring the permeability characteristics of highly porous media. J Hydrol. 2018;562:725–32.
65. Gavili A, Zabihi F, Dallali Isfahani T, Sabbaghzadeh J. The thermal conductivity of water base ferrofluids under magnetic field. Exp Therm Fluid Sci. 2012;41:94–8.
66. Mehrali M, Sadeghinezhad E, Akhiani AR, Tahan Latibari S, Simon H, Metselaar C, Kherbeet A. Heat transfer and entropy generation analysis of hybrid graphene/Fe_3O_4 ferro-nanofluid flow under the influence of a magnetic field. Powder Technol. 2017;308:149–57.
67. Abdel-wahed MS. Magneto hydrodynamic Ferro-Nano fluid flow in a semi-porous curved tube under the effect of hall current and nonlinear thermal radiative. J Magn Magn Mater. 2019;474:347–54.
68. Qin Y, He H, Ou X, Bao T, Experimental study on darkening water-rich mud tailings for accelerating desiccation. J Clean Product 118235. 2019. Doi: 10.1016/j.jclepro.2019.118235.
69. Sheikholeslami M. Numerical investigation for CuO–H_2O nanofluid flow in a porous channel with magnetic field using mesoscopic method. J Mol Liq. 2018;249:739–46.
70. Sheikholeslami Mohsen. Magnetic field influence on CuO-H_2O nanofluid convective flow in a permeable cavity considering various shapes for nanoparticles. Int J Hydrog Energy. 2017;42:19611–21.
71. Qin Y, Hiller JE, Meng D. Linearity between pavement thermophysical properties and surface temperatures. J Mater Civ Eng. 2019. https://doi.org/10.1061/(ASCE)MT.1943-5533.0002890.
72. Qin Y, Luo J, Chen Z, Mei G, Yan L-E. Measuring the albedo of limited-extent targets without the aid of known-albedo masks. Sol Energy. 2018;171:971–6.
73. Sheikholeslami M. Numerical investigation of nanofluid free convection under the influence of electric field in a porous enclosure. J Mol Liq. 2018;249:1212–21.
74. Sheikholeslami Mohsen. CuO-water nanofluid flow due to magnetic field inside a porous media considering Brownian motion. J Mol Liq. 2018;249:921–9.
75. Qin Y. A review on the development of cool pavements to mitigate urban heat island effect. Renew Sustain Energy Rev. 2015;52:445–59.
76. Sheikholeslami M, Shehzad SA. Magnetohydrodynamic nanofluid convection in a porous enclosure considering heat flux boundary condition. Int J Heat Mass Transf. 2017;106:1261–9.
77. Sheikholeslami M, Hayat T, Alsaedi A. Numerical study for external magnetic source influence on water based nanofluid convective heat transfer. Int J Heat Mass Transf. 2017;106:745–55.
78. Sheikholeslami M, Ellahi R. Three dimensional mesoscopic simulation of magnetic field effect on natural convection of nanofluid. Int J Heat Mass Transf. 2015;89:799–808.
79. Qin Y, He Y, Hiller JE, Mei G. A new water-retaining paver block for reducing runoff and cooling pavement. J Clean Prod. 2018;199:948–56.
80. Sheikholeslami M, Seyednezhad M. Nanofluid heat transfer in a permeable enclosure in presence of variable magnetic field by means of CVFEM. Int J Heat Mass Transf. 2017;114:1169–80.
81. Qin Y, Zhao Y, Chen X, Wang L, Li F, Bao T. Moist curing increases the solar reflectance of concrete. Constr Build Mater. 2019;215:114–8.
82. Qin Y, Zhang M, Hiller JE. Theoretical and experimental studies on the daily accumulative heat gain from cool roofs. Energy. 2017;129:138–47.
83. Sheikholeslami M. Solidification of NEPCM under the effect of magnetic field in a porous thermal energy storage enclosure using CuO nanoparticles. J Mol Liq. 2018;263:303–15.
84. Sheikholeslami M. Influence of magnetic field on Al2O3-H2O nanofluid forced convection heat transfer in a porous lid driven cavity with hot sphere obstacle by means of LBM. J Mol Liq. 2018;263:472–88.
85. Qin Y, He H. A new simplified method for measuring the albedo of limited extent targets. Solar Energy. 2017;157(Supplement C):1047–55.
86. Sheikholeslami M, Shehzad SA. Thermal radiation of ferrofluid in existence of Lorentz forces considering variable viscosity. Int J Heat Mass Transf. 2017;109:82–92.

87. Sheikholeslami M, Rokni HB. Nanofluid two phase model analysis in existence of induced magnetic field. Int J Heat Mass Transf. 2017;107:288–99.
88. Qin Y, He Y, Wu B, Ma S, Zhang X. Regulating top albedo and bottom emissivity of concrete roof tiles for reducing building heat gains. Energy Build. 2017;156(1):218–24.
89. Krishna Shah R, Khandekar S. Exploring ferrofluids for heat transfer augmentation. J Magn Magn Mater. 2019;475:389–400.
90. Hao T, Ma H, Ma X. Heat transfer performance of polytetrafluoroethylene oscillating heat pipe with water, ethanol, and acetone as working fluids. Int J Heat Mass Transf. 2019;131:109–20.
91. Sheikholeslami Mohsen, Vajravelu Kuppalapalle, Rashidi MM. Forced convection heat transfer in a semi annulus under the influence of a variable magnetic field. Int J Heat Mass Transf. 2016;92:339–48.
92. Wang L, Wang Y, Yan X, Wang X, Feng B. Investigation on viscosity of Fe_3O_4 nano-fluid under magnetic field. Int Commun Heat Mass Transf. 2016;475:23–8.
93. Phillips RJ. Micro channel heat sinks. Adv Thermal Model Electron Compon Syst. 1992;2:109–84.
94. Aminfar H, Mohammadpourfard M, Zonouzi SA. Numerical study of the ferrofluid flow and heat transfer through a rectangular duct in the presence of a non-uniform transverse magnetic field. J Magn Magn Mater. 2013;327:31–42.
95. Tzirtzilakis EE, Xenos MA. Bio-magnetic fluid flow in a driven cavity. Meccanica. 2013;48:187–200.